

NO_x production using pulsed atmospheric plasma discharge: Identification and diagnostics

Yiwei Jiang, Anton Nikiforov, Mikhail Gromov, Nathalie De Geyter, Rino Morent

Research Unit Plasma Technology (RUPT), Department of Applied Physics, Ghent University, Ghent, Belgium

Abstract: The synthesis of nitric oxides was studied using a pulsed atmospheric plasma discharge by measuring plasma discharge electrical characteristics and optical emission spectroscopy. The pulsed atmospheric plasma has unique features as revealed by the voltage and current measurements. The mass flow rate was found to have a significant influence on the discharge cycle period. Based on optical emission spectroscopy measurements, rotational and vibrational temperature of N₂ plasma was determined.

Keywords: Nitrogen fixation, NO_x production, pulsed plasma, optical spectroscopy

1. Introduction

As an essential constituent of all living organisms, nitrogen can be found in nucleic acids, amino acids and different kinds of enzyme. The abundance of nitrogen is obvious because it makes up 78% of the earth atmosphere. This abundance makes it an extremely promising and economical nitrogen source for the conversion of nitrogen from the air into “fixed forms” like nitrate NO₃⁻ or ammonia NH₃. However, its accessibility to plants and animals is not easy due to the difficulty in breaking the triple-bond of N≡N. Since the 20th century, with the growing demand for agriculture production, humans have been trying to capture nitrogen to produce fertilizers in different ways including chemical synthesis, biochemical conversion and plasma-assisted fixation.

In the past decades, interest has raised in studying the capability of thermal and non-thermal plasmas in different synthesis processes of ammonia or nitric oxide. Normally, the plasma used in these lab-scale reactors is non-thermal typically characterized by high chemical activity. Compared to the traditional chemical method – the Haber-Bosch process, non-thermal plasma has advantages associated with its green emission, small scale production and potential high energy efficiency [1]. For plasma assisted nitric oxide production, only air or N₂+O₂ mixture is needed, which means that there is no need for hydrogen produced in the hydrocarbon industry. Furthermore, reducing the usage of and dependency on hydrocarbons also caters to the energy planning for next generations.

Since the 1930s, various kinds of plasma reactors have been designed and applied for N₂ fixation. Peng et al. [2] categorize the different reactors, describe their most important features and compare their performance. Dielectric barrier discharge [3-5], gliding arc reactors [6-8] and plasma jets [9, 10] appear to be most often used in recent research. Without the assistance of catalysis, it seems hard for DBDs to crack the nitrogen bond with sufficient yield. Efforts on gliding arc reactors showed promising output with energy efficiency of 2.8 MJ/mol at high specific energy input of 2000 J/L [11], part of which, at the same time, was unfavorably wasted on gas heating. In this work, a pulsed discharge is utilized to generate active plasma in a pin-to-plate system. In terms of converting more energy into the plasma, a pulsed discharge

demonstrates itself as a better option due to its lower heating loss in slim and transient plasma filaments. The addition of water into pulsed discharge reactors was proved to be a good combination to produce aqueous nitrite and nitrate [12, 13]. So far, the research in such applications is still lacking. The motivation in our work is to develop a better understanding in this new type of plasma sources by electrical measurements and optical emission spectroscopy.

2. Experiment

2.1. Plasma source

The schematic diagram of the reactor system is shown in Fig. 1. The power subsystem includes a negative DC power supply (Glassman ER30) and the electrical circuit as illustrated in Fig.2. Current and voltage are measured by a current transformed monitor (Pearson™ Electronics model 2877) and a high voltage probe (Tektronix P6015A), both connected to an oscilloscope (LeCroy Wave Surfer 64Xs). Inside the reactor box, there is a stainless plate working as ground electrode and placed on top. Underneath, 14 pins, inserted in quartz gas tubes, stand in even distance. The adjustment of the gap between pins and plate has an impact on the plasma characteristics. In this paper, the gap is fixed at 5 mm. Equal distribution of air into each pin is able to reduce the discharge difference among pins since pins cannot be manufactured exactly the same. A silicon window is mounted for optical measurements, from which a fiber collects the emission signal of the plasma. The spectrometer (Avantes AvaSpec-3648) with a high resolution in wavelength regime (350-390nm) is used to process the spectral information. The exhausted gas is abductured into the ventilation system.

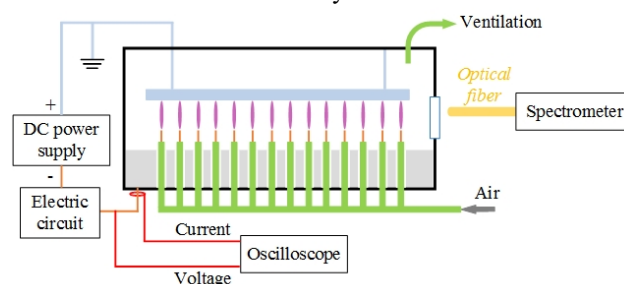


Figure 1 Schematic of the pulsed discharge system

The pulsed plasma is generated by the electrical circuit shown in Fig. 2. Two main capacitors (C1, 1.3 nF) are used as energy storage together with a resistor (R1, 1.8 k Ω) that limits the total current. When the voltage in C1 is high enough to break down the gas in the spark gap, plate discharges take place between pins and the ground and they are sustained by the parallel RC circuits (R2, 1 M Ω ; C2, 10 pF). Normally, the onset of pulsed plasma starts at -14kV.

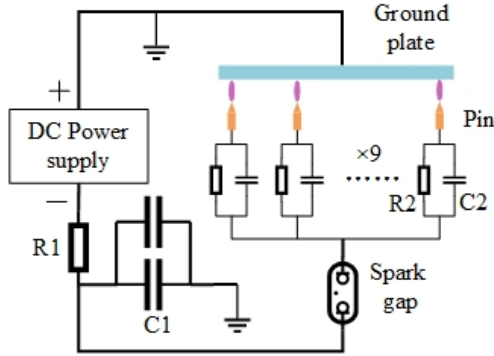


Figure 2 Electrical circuit of pulsed plasma generator

2.2. Spectrum processing methodology

Optical emission spectroscopy is a common technique employed in plasma diagnostics. Establishment of numerous analytical methods has paved the way for researchers to determine the plasma properties like plasma temperature, electron density and elemental composition of the gas phase. The main goal in this work is to obtain the relation between discharge conditions and plasma temperature. For this purpose, two analytical approaches are adopted to calculate the rotational and vibrational temperature of N₂ plasma, based on the emission of the second positive system (SPS) of N₂ (transition C³Π_u – B³Π_g, 546-268 nm).

Rotational temperature

The rotational temperature (T_{rot}) was calculated based on the use of the transition SPS N₂ with vibronic numbers $v''-v' = 0-2$, where v'' and v' indicate lower and upper states respectively. The corresponding band is located at the wavelength of 375-380.5 nm. Assuming that N₂ groups have a Boltzmann distribution, we can define T_{rot} from the slope of $-\alpha$ (y axis) versus $\ln(I/G)$ (x axis), in which α is a rotational term of the transition, I is the intensity of at specific rotational number J_i and $G_r(J)$ is rotational energy value (cm⁻¹). The details concerning the calculation of α , I , G have been discussed in Ref [14]. The linear fitting of $-\alpha$ versus $\ln(I/G)$ is also given in Fig. 3 (upper left), in which 13 points are chosen from J_i ($i=8,10,\dots,32$). It is obvious that two lines can be distinguished with different slopes thus resulting in two calculated temperatures, $T_1=470K$, and $T_2=1166K$. In this paper, only the lower temperature is regarded as the rotational temperature.

Vibrational temperature

In the second positive system of N₂, four peaks are selected to determine the vibrational temperature. As Fig 4 shows, these peaks are located at 367.1, 370.9, 375.4 and

380.4 nm, which correspond to vibrational transitions 3→5, 2→4, 1→3 and 0→2, respectively. After series processing of the measured intensity [14], terms including $\ln(I\lambda v''v'/Av''v')$ and G_v can be obtained. Linear fitting of them gives the slope $\tan(\beta)$ that is related to T_{vib} by $T_{vib} = 1/(k \cdot \tan(\beta))$ where k is a constant.

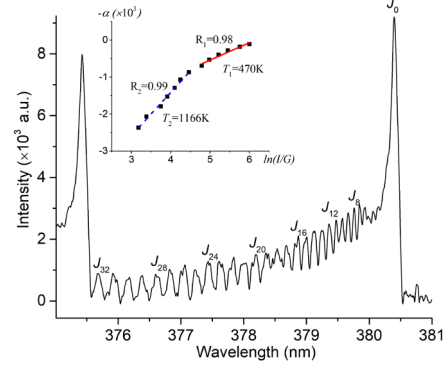


Figure 3 Rotational spectrum of N₂ in vibrational level 0→2 band, and linear fitting (upper left), $Q=10$ slm, $I_{total}=2$ mA

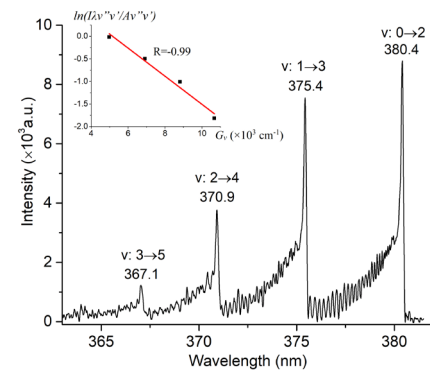


Figure 4 Typical spectrum of second positive system of N₂ and linear fitting (upper left), $Q=10$ slm, $I_{total}=2$ mA

3. Results and discussion

3.1 Electrical measurement

With a low sampling resolution (50 ms/div), the oscilloscope records the discharge voltage waveform within 0.5 second as shown in Fig. 5. The interval between peaks is defined as the discharge cycle period, which is not evenly distributed. Unstable discharge can be found around 0.05 s and 0.1 s mainly caused by the chaotic gas dynamics in the spark gap. In general, the pulsed plasma is stable in 90% of the total time.

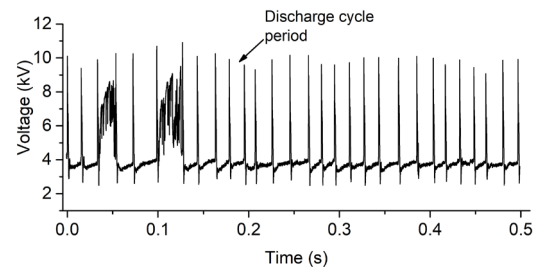


Figure 5 voltage waveform with sampling resolution 50ms/div, $Q=10$ slm, $I_{total}=3$ mA

By counting the number of intervals, average discharge periods can be calculated for a specific condition (3 times repetition). The variation of discharge period Δt is plotted in Fig. 6 as a function of flow rate. The fact that Δt reaches a maximum at =12 slm and that it then drops with flow rate may be attributed to the decreasing residence time of the gas in the discharge gap. In addition, the rising pressure inside the reactor at high flow rates facilitates streamer formation between pins and plate thus leading to a more frequent and stronger discharge with smaller Δt .

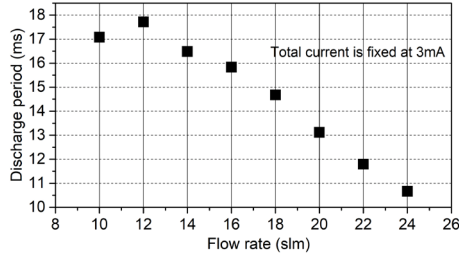


Figure 6 Discharge period as a function of flow rate, $I_{total}=\text{constant}$ (3mA)

With a higher sampling resolution, the voltage-current waveforms are shown in Fig. 7. The pulse lasts for about 350 ns while the current climbs to its peak (30.2 A) in only 8 ns. The interval between two dashed lines is picked for power calculation (integration). As a result, the main pulse consumes 33.6 mJ.

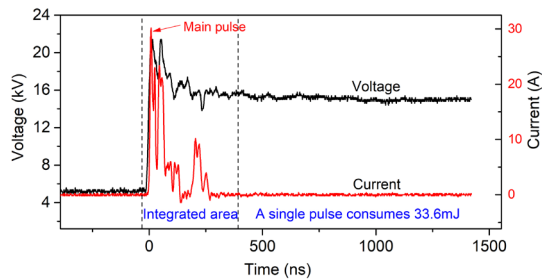


Figure 7 A main pulse of the 14-pin total current with sampling resolution 250 ns/div, $I_{total}=\text{constant}$ (3 mA), $Q=10$ slm

3.2 OES diagnosis

Normalization of the optical emission spectrum at different flow rates is demonstrated in Fig. 8. Calculation results of T_{rot} and T_{vib} (N_2) are listed in Table 1 and 2 for different flow rates as a function of total current. For rotational temperature, the increase of flow rates from 10 slm to 18 slm leads to higher T_{rot} with a maximum of 568 K at $Q=18$ slm, $I_{total}=3$ mA while T_{rot} drops at $Q=22$ slm. However, the big deviations in Table 1 imply that the actual T_{rot} maybe varies not significantly (around 525 K) for different conditions. In other words, flow rate and discharge current have negligible impact on T_{rot} . The variation of vibrational temperature as a function of current for different flow rates can be deduced from Table 2. The minimum value (5000 K) appears at $Q=10$ slm, $I_{total}=2$ mA and maximum (7340 K) at $Q=22$ slm, $I_{total}=2$ mA. Considering that vibrational excited nitrogen species play

a significant role in NO_x production [15], the high temperature implies that more nitric oxide will be observed in high flow rates, which needs further proof.

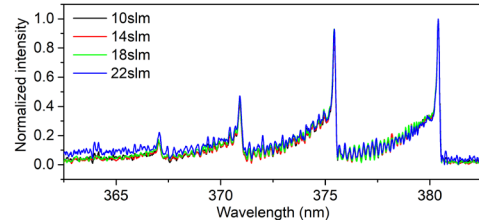


Figure 8 Optical emission spectrum at different flow rates, I_{total} is fixed at 3mA

Table 1 Rotational temperature (K) as function of discharge current for different flow rates

I_{total} / Q	2.0 mA	3.0 mA	4.0 mA
10 slm	475±38	484±41	483±40
14 slm	494±44	544±39	546±39
18 slm	556±44	568±45	500±51
22 slm	525±46	522±46	504±47

Table 2 Vibrational temperature (K) as function of discharge current for different flow rates

I_{total} / Q	2.0 mA	3.0 mA	4.0 mA
10 slm	5001±214	5031±202	5178±179
14 slm	5033±164	5132±212	5147±214
18 slm	5767±198	5836±201	5516±189
22 slm	7342±566	6993±562	6624±391

4. Conclusion

This paper discusses the electrical and optical characterization of a pulsed plasma reactor used for nitrogen fixation. The above analysis shows that the discharge period decreases with increasing air flow rate. Peak current can reach 30.2 A in a main pulse, which corresponds to an energy consumption of 33.6mJ. From optical emission measurements, flow rate is found to have no or little influence on the rotational temperature of N_2 . In contrast, the impact of gas flow rate on the vibrational temperature of N_2 is very important.

Acknowledgement

The authors want to acknowledge the funding support from the NITROPLASM project (FWO-F.R.S./FNRS EOS ref.n.° 30505023) and the China Scholarship Council.

References

- [1] V. Hessel, et al. Chem. Eng. Process. **71**, (2013)
- [2] P. Peng, et al. J. Clean Prod. **177**, (2018)
- [3] B.S. Patil, et al. Applied Catalysis B: Environmental. **194**, (2016)
- [4] X. Tang, et al. Plasma Chem. Plasma Process. **38**, 3 (2018)
- [5] Y. Han, et al. Plasma Science and Technology. **20**, 1 (2018)

- [6] B.S. Patil, et al. *AIChE J.* **64**, 2 (2018)
- [7] J. Yang, et al. *J. Electrochem. Soc.* **163**, 10 (2016)
- [8] B.S. Patil, et al. *Plasma Chem. Plasma Process.* **36**, 1 (2015)
- [9] Y. Mizukoshi, et al. *Chem. Lett.* **44**, 4 (2015)
- [10] P. Peng, et al. *Chem Commun (Camb)*. **54**, 23 (2018)
- [11] W. Wang, et al. *ChemSusChem*. **10**, 10 (2017)
- [12] W. Bian, et al. *J. Electroanal. Chem.* **70**, 3 (2012)
- [13] W. Bian, J. Shi, and X. Yin. *IEEE Trans. Plasma Sci.* **37**, 1 (2009)
- [14] G. Herzberg, *Molecular Spectra and Molecular Structure* Vol. 1. (2013)
- [15] V.D. Rusanov, A.A. Fridman, and G.V. Sholin. *Sov. Phys. Usp.* **24**, 6 (1981)